Prediction of Volatile Anesthetic Binding Sites in Proteins

John H. Streiff,* Thomas W. Allen,† Elena Atanasova,† Nenad Juranic,‡ Slobodan Macura,‡ Alan R. Penheiter,* and Keith A. Jones*

Departments of *Anesthesiology and †Molecular Pharmacology and Experimental Therapeutics and ‡Biochemistry and Molecular Biology, Mayo College of Medicine, Rochester, Minnesota

ABSTRACT Computational methods designed to predict and visualize ligand protein binding interactions were used to characterize volatile anesthetic (VA) binding sites and unoccupied pockets within the known structures of VAs bound to serum albumin, luciferase, and apoferritin. We found that both the number of protein atoms and methyl hydrogen, which are within ~8 Å of a potential ligand binding site, are significantly greater in protein pockets where VAs bind. This computational approach was applied to structures of calmodulin (CaM), which have not been determined in complex with a VA. It predicted that VAs bind to $[Ca^{2+}]_4$-CaM, but not to apo-CaM, which we confirmed with isothermal titration calorimetry. The VA binding sites predicted for the structures of $[Ca^{2+}]_4$-CaM are located in hydrophobic pockets that form when the Ca^{2+} binding sites in CaM are saturated. The binding of VAs to these hydrophobic pockets is supported by evidence that halothane predominantly makes contact with aliphatic resonances in $[Ca^{2+}]_4$-CaM (nuclear Overhauser effect) and increases the Ca^{2+} affinity of CaM (fluorescence spectroscopy). Our computational analysis and experiments indicate that binding of VA to proteins is consistent with the hydrophobic effect and the Meyer-Overton rule.

INTRODUCTION

Volatile anesthetics (VA) are small hydrophobic molecules used to induce general anesthesia. A thorough understanding of the mechanisms by which these drugs induce anesthetic effects remains elusive, especially at the cellular level. Thus, continued study of the molecular mechanisms of anesthetic effects is warranted.

VAs interact with many cellular components, yet anesthetic effects ultimately manifest as changes in protein function. VAs have been shown to accumulate at the aqueous interface of a dipalmitoylphosphatidylcholine membrane (1) and at the protein-lipid interface region near the surface of purple membrane (2). VAs are known to bind to transmembrane proteins such as the plasma membrane Ca^{2+}-ATPase (3), rhodopsin (4), the nicotinic acetylcholine receptor (5,6), and several proteins from rat neuronal membranes, assayed in vitro (7). VAs also alter the function of several membrane-delimited proteins such as the G-protein-coupled muscarinic receptor complex (8) and the Ca^{2+}-ATPase pump (9). However, a lipid environment is not essential for anesthetic-protein interactions. VAs are known to bind to soluble proteins such as serum albumin (10), apoferritin (11), odorant binding protein (12), firefly luciferase (13), and calmodulin (14). VAs have been shown to inhibit the normal function of luciferase (15) and such soluble mammalian proteins as Protein kinase C (16–18) and multiple isoforms of G-protein alpha subunits (19), which may be relevant to the anesthetic mechanism. Together, these findings suggest that proteins are potential molecular targets of anesthetics.

Protein structure affects the affinity and stoichiometry with which VAs bind. VAs bind to some proteins, such as apoferritin (11), serum albumin (10), and odorant binding protein (12), with dissociation constants (K_d) of ~1 mM and above, yet do not bind to other proteins even when present at 10-fold higher concentrations (unpublished observations). This suggests that VAs, when present at mM concentrations, bind to some, but not all proteins. This was also observed in the cellular environment, when the binding of VAs to proteins from rat neuronal membranes was assayed in vitro (7). In addition, this work suggests that VA binding to proteins in the cellular environment is affected by protein conformation. Conformational dependent binding of VAs to proteins has also been observed using purified, isolated proteins. It has been shown that VAs bind to apomyoglobin, but not myoglobin (14,20) and Ca^{2+}-saturated calmodulin, but not Ca^{2+}-free calmodulin (14). This suggests that VAs bind preferentially to certain protein conformations. In some proteins, such as serum albumin, some binding interactions are saturable at VA concentrations achievable in aqueous environments (21). VA binding has also been shown to compete with native ligands of some proteins, such as fatty acid binding to serum albumin (21,22) and the binding of the firefly luciferase substrate luciferin (23). Thus, these findings indicate that VAs bind to some, but not all proteins. VAs bind preferentially to certain protein conformations, and VAs are able to compete with certain protein ligands. Together, this suggests that VAs bind specifically to structures within certain proteins and protein assemblies.

High resolution structures of VA·protein complexes formed between bromoform·luciferase (13), halothane·human serum albumin (22), and halothane·apoferritin and isoflurane·apoferritin (11) were determined by other groups. In these

Submitted February 2, 2006, and accepted for publication July 13, 2006.

Address reprint requests to J. H. Streiff, Tel.: 507-284-1342; E-mail: streiff.john@mayo.edu.

0006-3495/06/11/3405/10 $2.00

doi: 10.1529/biophysj.106.082586

works, it was found that VAs bind to preexisting pockets lined with polar and apolar residues, which exist within protein monomers and between oligomeric protein complexes; binding was consistent with the hydrophobic effect, yet the halogen atoms of the VAs may have weak polar interactions with the protein, and the bound anesthetics induced minor changes in protein structure. Thus, the structures of complexes formed between VAs and proteins, which themselves are not physiologically relevant anesthetic targets, provide detailed information about the molecular interactions and protein motifs that influence the binding of VAs to proteins in general.

The main goal of this work is to correlate VA binding with protein structure. Our use of computational tools, which are designed to predict and visualize ligand binding pockets in protein structures, is a novel aspect to this investigation. This approach is applied to calmodulin (CaM), the structure of which has not been determined in complex with VAs, and empirical evidence supporting the predictions is provided. CaM was studied because both the apo- and $[Ca^{2+}]_4$-CaM structures (24–26) can be utilized to investigate the structure-dependent specificity for VA binding, which is inferred from NMR experiments (14).

METHODS

CaM expression, enrichment, and purification

Human calmodulin cDNA was subcloned into pET-15b expression vector (Novagen, San Diego, CA) using standard cloning techniques. No purification tag was introduced into the construct. The identity of the insert was confirmed by DNA sequencing. CaM was overexpressed in BL21(DE3)-pLysS strain of *Escherichia coli* (Single Shot, Novagen, San Diego, CA). Uniform ^{13}C, ^{15}N enrichment was achieved by growing cells in Luria-Bertani medium and then inducing in minimal media containing ^{13}C-glucose and $^{15}NH_4Cl$ following established protocols (27). Isotopically labeled and unlabeled CaM were purified using a slight modification to an existing procedure (28). Five mM $CaCl_2$ was added to the cleared cell lysate, which was loaded onto a phenyl-Sepharose CL-4B column (Sigma, St. Louis, MO), and the CaM was eluted with 1 mM EGTA. CaM fractions were further purified using a HiTrap Q column (Amersham Biosciences, Uppsala, Sweden) and a 0–1 M NaCl gradient. CaM was >95% pure, judging by SDS-gel electrophoresis and Coomassie Brilliant-Blue staining. The identity of the CaM was confirmed by N-terminal sequencing as well as by LC-MS analysis of the tryptic digests of labeled and unlabeled CaM. The molecular weight and labeling efficiency (96%) were verified with ESI-MS by direct infusion.

Isothermal titration calorimetry

Isothermal titration calorimetry (ITC) was used to estimate the thermodynamic parameters (stoichiometry (n), dissociation constant (K_d), and enthalpy (ΔH)) of halothane $[Ca^{2+}]_4$–CaM binding. We were concerned that it would be difficult to determine these parameters for VA-protein interactions from a single ITC experiment because it might require very high protein concentrations (29). Therefore, the binding isotherms were measured for several concentrations of protein and the n, K_d, and ΔH determined as parameters from a global fit to the set of binding isotherms (30). In the experiments, the heat associated with a series of 10 μL injections (30 total) of a near-saturated solution of halothane (quantified by gas chromatography (31)) into a solution of various concentrations of calmodulin dissolved in the same buffer were measured using a VP-ITC microcalorimeter (Microcal, Northampton, MA). The heats associated with diluting the protein and halothane were measured in separate experiments by injecting buffer into the cell-containing protein and by injecting halothane into the cell-containing buffer, respectively. These heats were subtracted from the heat of halothane·protein binding. Measurements of halothane·$[Ca^{2+}]_4$–CaM binding were performed in 100 mM KCl and 6.2 mM $CaCl_2$ (pH 7) and the measurement of halothane·apoCaM binding was performed in 100 mM KCl, 1 mM EDTA, and 1 mM EGTA (pH 7). The binding isotherms were constructed by plotting the integrated heat versus the halothane: protein mole ratio for five concentrations of CaM from 0.01 to 0.69 mM. The binding isotherms were fit to a single site model (32), which allowed for more than one halothane binding site in the protein, but assumed that all sites had equivalent K_d. We tested this approach using BSA and estimated that halothane binds with a stoichiometry of 3, an apparent K_d of 1.8 mM, and a $\Delta H = -4.0$ Kcal/mol (data not shown). These results are consistent with values for VA binding to serum albumin determined by others using ITC, NMR, and fluorescence techniques (10,33,34). This finding suggests that this approach could provide a reasonable estimate of n, K_d, and ΔH for halothane binding to CaM.

CaM Ca^{2+} K_d values

The K_d values of the Ca^{2+} binding sites of CaM were determined using fluorescence spectroscopy. The intrinsic Tyr fluorescence (excitation 277 nm, emission 320 nm) increases threefold when Ca^{2+} saturates the two Ca^{2+} binding sites of the C-domain (35). Tyr residues in the C-domain can be used to monitor the Ca^{2+} binding to the C-domain sites without interference from Phe residues in the N-domain ((35) and references therein). The intrinsic phenylalanine fluorescence (excitation 250 nm, emission 280 nm) decreases by ~30% when Ca^{2+} saturates the two Ca^{2+} binding sites on the N-domain (36). At these excitation and emission frequencies, the Phe residues in the N-domain report exclusively on the Ca^{2+} occupancy of N-domain sites. There is no contribution to the signal from the Phe residues in the C-domain, no spectral interference from the Tyr residues in the C-domain, and no observable energy transfer from the Phe residues in the N-domain to the Tyr residues in the C-domain (35). Samples of 5 μM CaM in 50 mM MOPS (pH 7.2), 100 mM KCl, 5 mM nitriloacetic acid, and 50 μM EGTA were prepared in quartz cells sealed with Teflon stoppers, and stirred with Teflon-coated micro stir bars. Small aliquots of a calcium stock solution were added with a syringe through a port in the Teflon stopper. After each addition, the solution was stirred for 2 min and the fluorescence was recorded using a thermostatically controlled Spex Fluoromax fluorometer (Jobin Yvon, Edison, NJ) with the slits set to 2 nm bandpass. Free Ca^{2+} in the fluorescence titrations was determined with the fluorescent probe Oregon Green 488 BAPTA-5N (Molecular Probes, Eugene, OR), which was calibrated using standardized Ca^{2+} solutions (Molecular Probes). Immediately after the titration, an aliquot of the solution was removed for halothane concentration determination by gas chromatography (31). The normalized fluorescence change $F = (F_i\text{-}F_{min})/(F_{max}\text{-}F_{min})$ for the tyrosine and phenylalanine residues were plotted as a function of free Ca^{2+} concentration and fit with the following equation (37):

$$F = \frac{[Ca^{2+}]^n}{[Ca^{2+}]^n + K_d^n}. \quad (1)$$

K_d is the dissociation constant, $[Ca^{2+}]$ is the free Ca^{2+} concentration, and n is the Hill coefficient. Each titration was performed in triplicate and each titration curve was fit to Eq. 1. The curve-fit parameters for each set of triplicate experiments were expressed as mean ± SD in Table 3.

Halothane is a poor quencher of Tyr and Phe emission in CaM (Tyr < 5% and Phe < 15% at 2.5 mM). The quenching of the emission was not corrected because each titration was performed at constant halothane concentrations and the degree of quenching was the same for apo- and

$[Ca^{2+}]_4$-CaM conformations (data not shown). The magnitude of the changes in the Phe and Tyr emission intensities between apo- and $[Ca^{2+}]_4$-CaM were also insensitive to halothane concentrations up to 2.5 mM (data not shown). This suggests the experimental conditions do not create a significant amount of chlorotrifluoroethy radical (38) or that any chlorotrifluoroethy radical that cross-links with CaM does not affect the emission intensities of Phe or Tyr and hence the assay.

NMR spectroscopy

The NOESY spectrum (39) of 2 mM CaM in 25 mM HEPES (pH 7.5), 100 mM KCl, 20 mM Ca^{2+}, 5 mM Mg^{2+}, 1 mM EDTA, and 4 mM halothane was recorded at 298 K and a mixing time of 300 ms using a 600 MHz spectrometer equipped with a cryoprobe (Bruker, Billerica, MA).

Characterization and prediction of VA binding sites

High resolution structures of VA·protein complexes deposited in the Protein Data Bank (40) were analyzed for protein motifs that influenced VA binding. The protein structures were HSA (1E7C (22)), luciferase (1BA3 (13)), and the apoferritin dimer (chains B and E from 1IES (41)). The coordinates of the bound VAs around HSA were determined from a composite of 1E7B and 1E7C (22); around luciferase from 1BA3 (13); and around apoferritin from 1XZ3 (11). Visual molecular dynamics (VMD) (42) and associated programs were used to add hydrogen atoms to the proteins and solvate them in a box of water at least 10 Å larger than the protein in all directions. NAMD (43) was used to minimize the solvated protein structures.

The program Putative Active Sites with Spheres (PASS) (44) was used to define VA binding site predictions (BSPs) for the minimized protein structures. PASS is designed to predict the site(s) in protein structures where small hydrophobic molecules prefer to bind. The PASS algorithm fills pockets in protein structures with virtual probe spheres, which are assigned a burial count (BC) equal to the number of protein atoms within 8 Å. The probe weight of the i^{th} sphere (PW_i) is calculated (Eq. 2) as the sum of the burial counts of all spheres, which are scaled by an envelope function:

$$PW_i = \sum_{j=1}^{Nprobes} BC_j \times e^{-(r_{ij}-2)^2}. \quad (2)$$

The envelope function attenuates the burial count of the j^{th} sphere using a function of its distance from the i^{th} sphere (r_{ij}). The envelope function is equal to 1 when $r_{ij} \leq 2$ Å and decays exponentially to 0 when $r_{ij} \geq 4.5$ Å. Thus BC of spheres $>\sim$4.5 Å from the i^{th} sphere contribute little to PW_i. *PW* is a measure of the hydrophobicity of the region surrounding the BSP even though it is a function of all nearby protein atoms, regardless of whether they are constituents of polar or nonpolar residues/functional groups. The rationale is that the deeper a pocket is buried in the protein, the more hydrophobic it is likely to be. Thus, the structure of the protein pocket is reduced to a number (*PW*), which PASS uses to rank the hydrophobicity of the BSP. Note that *PW* is an absolute scale on which all proteins can be compared. The probe with the largest *PW* (most buried) is the initial BSP defined for a protein structure. Subsequent BSPs are defined in order of decreasing PW using those probes, which are not within 8 Å of a prior BSP.

We modified the PASS algorithm to also calculate methyl burial counts, which are equal to the number of methyl hydrogen atoms within 8 Å of the probe, and methyl probe weights (PW_Ms), which were calculated by substituting the methyl burial counts for BC in Eq. 2. This way we can directly compare *PW* and PW_M, because they have the same dimensions. All methyl hydrogen atoms were taken into account: Ala (H^{β}), Val (H^{γ}), Leu (H^{δ}), Ile ($H^{\gamma 2}$ and H^{δ}), Met (H^{ε}), and Thr ($H^{\gamma 2}$). The modified PASS algorithm defined the initial BSP as the probe with the largest PW_M for a protein structure. Subsequent BSPs are defined in order of decreasing PW_M using those probes, which are not within 8 Å of a prior BSP. We iteratively define BSPs in this way until all probes are exhausted. The coordinates of BSPs were similar, whether they were ranked by *PW* (PASS) or PW_M (modified PASS), because the two values are interdependent. The BSPs determined by the modified PASS along with the associated *PW* and PW_M values were used in the subsequent work.

BSPs were categorized as occupied if they were within 3 Å of a VA molecule in the crystal structure of the VA·protein complex, fatty-acid-displaceable if they were within 3 Å of a myristate ligand in the structure of the HSA·halothane complex, or unoccupied if they were >3 Å from either. The halothane·HSA structures were determined under two different conditions. For 1E7B, an HSA crystal was exposed to 2.5 mM halothane and for 1E7C, an HSA·myristate crystal was exposed to 10 mM halothane. The myristate ligands in 1E7C might be obscuring sites that would otherwise be occupied by VAs. Rather than categorize them as unoccupied, they are categorized as fatty-acid-displaceable.

We used VMD and a probe radius of 1.4 Å to calculate the solvent-accessible surface area (SASA) of the aliphatic (Gly, Ala, Val, Leu, Ile, and Pro), aromatic (Phe, Tyr, and Trp), sulfur-containing (Met and Cys), alcohol (Ser and Thr), acidic (Asp and Glu), basic (His, Lys, and Arg), and amide (Asn and Gln) residue types within 8 Å of the BSPs. In addition, we calculated the SASA of those residues containing at least one methyl functional group (Ala, Val, Leu, Ile, Met, Thr) within 8 Å of the BSPs.

Prediction of VA binding sites in CaM

BSPs were defined for the structures of apoCaM (1QX5, (24)), $[Ca^{2+}]_4$–CaM in extended conformation (1CLL (25)), and $[Ca^{2+}]_4$-CaM in compact conformation (1PRW (26)). BSPs in the CaM structures with *PW* and PW_M that exceeded the corresponding mean values of *PW* and PW_M of the unoccupied sites in the structures of VA·protein complexes by $>\pm 1.5$ SD, were considered to be potential VA binding sites.

Statistics

Data are presented as mean ± SD. Significance was determined by unpaired *t*-test.

RESULTS

Volatile anesthetics bind to specific pockets in proteins

There are a total of eight halothane found in the halothane·HSA structures. Of the 60 BSPs for HSA, six are occupied by one or more VAs and seven are fatty-acid-displaceable. There are two bromoforms observed in the bromoform·luciferase structure, and of the 33 BSPs for luciferase, two are occupied. There is a single isoflurane in the isoflurane·apoferritin structure, which occupies one of the 24 BSPs for the apoferritin dimer.

The mean SASAs calculated for various residue types within 8 Å of the BSPs are listed in Table 1. The SASAs of aliphatic residues and residues containing at least one methyl functional group were significantly greater around occupied BSPs compared to unoccupied BSPs. There was not a significant difference between the SASAs of other residue types around occupied versus unoccupied BSPs.

The mean values of *PW* and PW_M for all BSPs are tabulated according to category (Table 2) and are significantly greater for occupied than unoccupied BSPs. The two

TABLE 1 Solvent-accessible surface areas (mean ± SD) of various residue types around unoccupied, occupied, and fatty-acid-displaceable BSPs

Residue type	Unoccupied (100)	Occupied (9)	Fatty acid displaceable (7)
Aliphatic*	440 ± 210	760 ± 110	780 ± 120
Containing $-CH_3$*	420 ± 200	740 ± 120	760 ± 70
Aromatic	190 ± 170	180 ± 190	360 ± 240
Containing sulfur	50 ± 100	0 ± 0	80 ± 110
Alcohols	140 ± 150	150 ± 150	60 ± 110
Acids	240 ± 180	180 ± 240	60 ± 110
Bases	350 ± 160	400 ± 160	270 ± 110
Amides	130 ± 160	60 ± 110	40 ± 110

The number of BSPs in each category is given in parentheses and the areas are expressed in units of $Å^2$.
*Significant difference ($p < 0.01$) between occupied and unoccupied.

data sets were partially resolved using a scatter plot of their PW and PW_M (Fig. 1 *A*).

BSPs are defined for the structures of apoCaM and both extended and compact conformations of $[Ca^{2+}]_4$-CaM. The BSPs defined for the apoCaM structure had PW and PW_M values characteristic of unoccupied sites whereas some BSPs defined for the $[Ca^{2+}]_4$-CaM structures had PW and PW_M values characteristic of an occupied site (Fig. 1 *B*). The BSPs with PW and PW_M values characteristic of an occupied site are all located within the hydrophobic pockets used in target recognition and binding in the $[Ca^{2+}]_4$-CaM structures (Fig. 2).

Volatile anesthetics bind to hydrophobic sites in $[Ca^{2+}]_4$-CaM, but not apoCaM

Isothermal titration calorimetry (ITC) was used to confirm that halothane binds to $[Ca^{2+}]_4$-CaM, but not apoCaM (Fig. 3) and to estimate that halothane binds to $[Ca^{2+}]_4$-CaM with n of 1.5, K_d of 1.1 mM, ΔH of -4200 cal mol^{-1}, and a ΔS of -0.5 cal mol^{-1} K^{-1} (Fig. 4). Halothane concentrations exceeding the K_d were used in all experiments to optimize the occupation of the binding site(s).

The Ca^{2+}-dependence of intrinsic CaM fluorescence was used to show that 2.5 mM halothane significantly decreases the Ca^{2+} K_d of the N-domain Ca^{2+} binding sites of CaM from 7.4 to 5.1 μM and the C-domain Ca^{2+} binding sites from 1.5 to 0.77 μM (Fig. 5 and Table 3).

TABLE 2 BSP weights (mean ± SD) calculated for unoccupied, occupied, and fatty-acid-displaceable BSPs

Weights	Unoccupied	Occupied	Fatty acid displaceable
PW*	800 ± 400	2000 ± 300	1500 ± 300
PW_M*	200 ± 100	700 ± 200	600 ± 200

The number of BSPs in each category is the same as in Table 1.
*Significant difference ($p < 0.01$) between occupied and unoccupied.

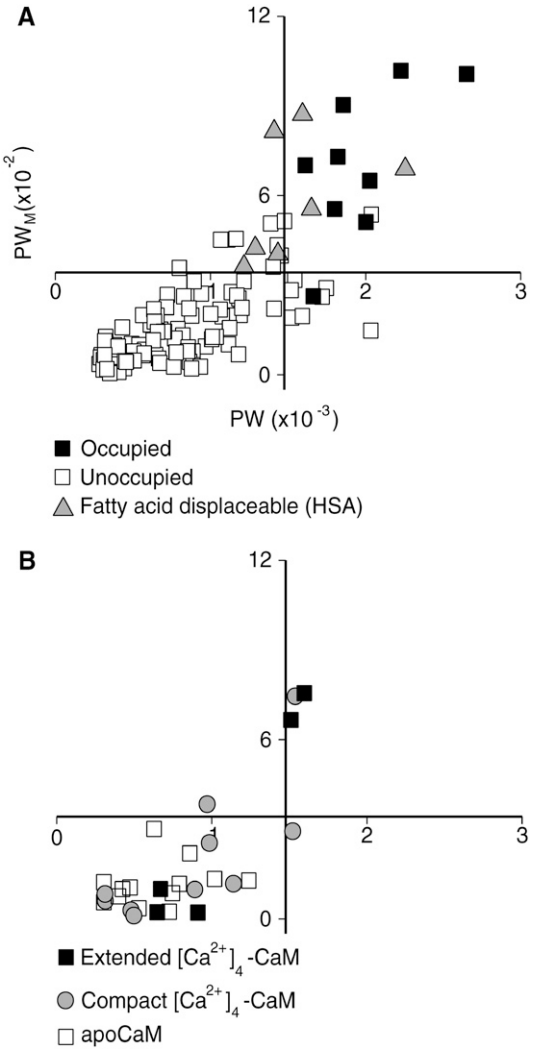

FIGURE 1 Scatter plots of BSPs. (*A*) Scatter plot of the occupied, unoccupied, and fatty-acid-displaceable BSPs. (*B*) Scatter plot of the BSPs for apoCaM and extended and compact $[Ca^{2+}]_4$-CaM. The axes in both plots are drawn to the same scale.

Multiple ^{1}H resonances of $[Ca^{2+}]_4$-CaM are observed predominantly between 0 and 3 ppm and to a lesser extent between 6 and 8 ppm in the one-dimensional slice from a NOESY spectrum taken at the halothane ^{1}H resonance frequency of 6.3 ppm (Fig. 6).

DISCUSSION

The main finding of this work is that VAs occupy pockets with significantly larger PW and PW_M than other potential binding sites in the structures of HSA, luciferase, and apoferritin. PW and PW_M are quantitative descriptors of the components of protein structure that influence VA binding. Using these descriptors, it is possible to compare the diverse structures of VA binding sites observed in the various VA·protein complexes using a common scale. These descriptors

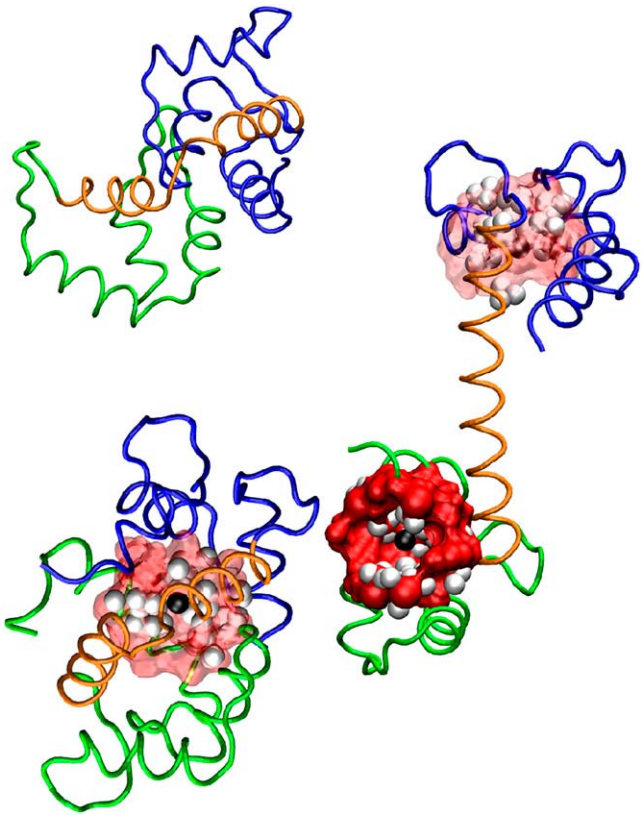

FIGURE 2 CaM structures used to determine BSPs. For clarity, the N-terminal domain (up to residue 65) is blue, the linker region (residues 66–92) is orange and the C-terminal domain (residues 93 and above) is green in each representation. (*Upper left*) No BSPs in the occupancy range were determined for apoCaM. (*Lower left*) A single BSP in the occupancy range (*solid black sphere*) was determined for $[Ca^{2+}]_4$-CaM in the compact conformation. The methyl hydrogen atoms within 8 Å of the BSP are represented as white spheres. All other atoms within 8 Å of the BSP are represented with a transparent red surface so they do not obscure the methyl hydrogens and BSP. (*Right*) Two BSPs in the occupancy range were determined for $[Ca^{2+}]_4$-CaM in the extended conformation. The BSPs are represented as for compact $[Ca^{2+}]_4$-CaM, except that the non-methyl hydrogen atoms within 8 Å of the BSP in the C-terminal domain are represented with a solid red surface to show the surface features of the pocket.

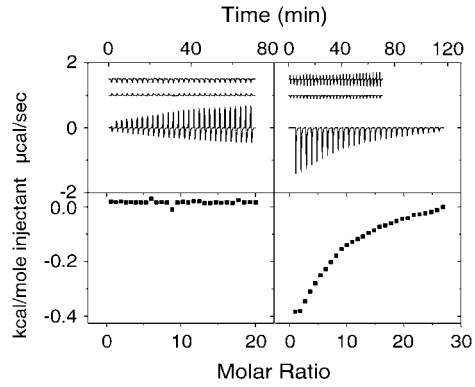

FIGURE 3 Titration of 100 μM apoCaM (*left*) and 100 μM $[Ca^{2+}]_4$-CaM (*right*) with halothane. The upper panels show the baseline-corrected data for the injection of halothane into buffer (*top trace*), the injection of buffer into calmodulin (*middle trace*), and the injection of halothane into calmodulin (*bottom trace*). The bottom panels show the normalized heat changes for each injection in calories per mole of halothane added, which were corrected for the enthalpies of dilution of halothane and calmodulin. The dilutions of halothane and $[Ca^{2+}]_4$-CaM (*upper right panel*) were collected with a shorter interval between injections than the titration of $[Ca^{2+}]_4$-CaM with halothane, which did not affect the subtraction of dilution enthalpies.

can be used to predict the site(s) of VA binding in protein structures, which could be a powerful tool for the study of molecular mechanisms of anesthesia.

Examination of the residues surrounding the BSPs indicated that the mean SASAs of aliphatic residues and those residues containing methyl groups were significantly greater for occupied BSPs compared to unoccupied BSPs (Table 1). The significance was approximately equivalent for either the aliphatic residues or the residues containing methyl groups. This suggests that the number of methyl groups around the BSP can be used as an indicator of VA binding. On the other hand, we did not find any correlation between BSP occupancy and the SASA of any other polar or apolar residue types. Thus we could not discern any other indicators of VA binding from this data set. Together, this suggests that the hydrophobicity of the pocket around the BSP has greater influence over the binding of VAs than the aromaticity or polarity of the pocket. Others have also suggested that the binding of VAs to protein targets is determined primarily by hydrophobic and van der Waals forces (45). However, there are too few structures to rule out the influences of aromatic or polar residues or the effect of pocket geometry and orientation on VA binding. Additional structures of VA·protein complexes are needed to refine this method because VAs may bind to other members of the proteome through interactions and at sites significantly different than observed in these complexes.

VA binding sites are partially resolved from unoccupied pockets using a scatter plot of PW and PW_M (Fig. 1). In the scatter plot, the ordinate and abscissa axes bisect the means of the occupied and unoccupied data, such that they are spaced at equivalent standard deviation intervals from both means ($\sim\pm1.5$ SD). The occupied BSPs are predominantly located in quadrant I (quadrants are numbered counterclockwise, starting from *upper right*). The exception to this is the occupied BSP corresponding to the bromoform molecule that binds to firefly luciferase through mainly polar interactions (13), which is located in quadrant IV. Unoccupied BSPs are found predominantly in quadrant III. The fatty-acid-displaceable BSPs defined for HSA could not be categorized as occupied or unoccupied, so their PW and PW_M values were excluded from the statistical analysis. They are predominantly found in quadrants I and II. It has been shown that fatty acids inhibit some VA binding to serum albumin (21), so it is possible that VAs also bind to some of these sites. Thus VA binding sites in the structures of VA·protein complexes, including those that might be obscured by fatty acids in HSA, correlate with the PW and PW_M.

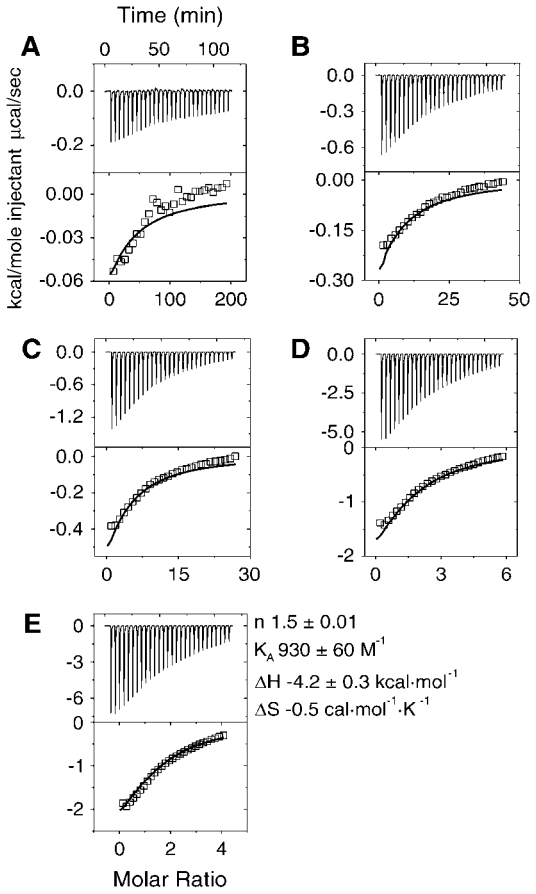

FIGURE 4 Titrations of various concentrations of $[Ca^{2+}]_4$-CaM with halothane. The halothane concentrations of the injectant were between 9 and 12 mM and the $[Ca^{2+}]_4$-CaM concentrations are 0.01, 0.05, 0.1, 0.5, and 0.69 mM in panels *A–E*, respectively. The upper panels show the baseline-corrected data for the injection of halothane into $[Ca^{2+}]_4$-CaM. The lower panels show the normalized heat changes for each injection in calories per mole of halothane added, which were corrected for the enthalpies of dilution of halothane and calmodulin. The solid line overlaid on the integrated heats is the simulated single-site-model binding isotherm calculated with parameters determined from a global fit to all five data sets. The thermodynamic parameters from the global curve fits are tabulated along with the standard errors of the fit, as determined by the fitting program.

PW is proportional to the number of nearby protein atoms and hence the exclusion of the binding site from the bulk solvent. The mean *PW* of the occupied BSPs was more than twice that of the unoccupied BSPs. This suggests that VA·protein complex formation is promoted by the desolvation of the VA (hydrophobic effect). However, the exothermic VA protein binding observed with titration calorimetry (Fig. 3 and in (12,29,46)) indicates that it is not the only force driving VA protein binding.

PW_M is proportional to the number of nearby methyl hydrogen and thus is related to the hydrophobicity of the binding site. The mean PW_M of occupied BSPs was more than threefold greater than that of the unoccupied BSPs. The preference of VAs for domains rich in methyl groups is consistent with NMR experiments, which demonstrate that

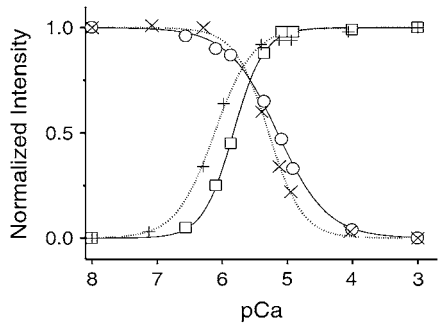

FIGURE 5 Effect of halothane on Ca^{2+} K_d of CaM. Representative titration curves of normalized fluorescence intensity change for tyrosine and phenylalanine measured in the presence and absence of 2.5 mM halothane. The graph symbols for the control tyrosine data are open squares, control phenylalanine data are open circles, halothane tyrosine data are + signs, halothane phenylalanine data are ***X***, control curvefits are solid lines, and halothane curvefits are dashed lines.

halothane contacts predominantly aliphatic and aromatic residues in HSA (47) and the VA methoxyflurane exclusively contacts the choline methyl group in dipalmitoylphosphatidylcholine micelles (1). This indicates that VA binding correlates with the hydrophobicity of the pockets and is consistent with the Meyer-Overton rule (48,49), which states that anesthetic potencies correlate with partition coefficients between aqueous and hydrophobic phases. This rule has been interpreted to indicate that membranes are critical for anesthetic effects. However, these findings suggest that hydrophobic domains within proteins are also potential anesthetic targets.

These findings are consistent with NMR measurements, which demonstrated that small hydrophobic organic molecules bind to hydrophobic cavities with low water occupancy in the protein lysozyme (50). This suggests that the binding of VAs and other small hydrophobic molecules with proteins may arise from a set of common molecular interactions.

These findings are compelling because they indicate that the definition of hydrophobic in the Meyer-Overton rule can be further narrowed and quantified in protein targets to mean pockets with a minimum degree of solvent exclusion and a minimum number of residues that contain methyl groups. This is an important finding, because hydrophobicity is

TABLE 3 Ca^{2+} titration curvefit parameters (mean ± SD of fits to three titrations)

Parameter	N-domain Ca^{2+} binding sites		C-domain Ca^{2+} binding sites	
Halothane (mM)	0	2.5	0	2.5
K_d (μM)*†	7.4 ± 0.3	5.1 ± 0.1	1.50 ± 0.04	0.77 ± 0.04
n	1.4 ± 0.2	1.7 ± 0.1	1.8 ± 0.1	1.5 ± 0.1

*Significant difference ($p < 0.01$) between N-domain Ca^{2+} binding sites measured in 0 and 2.5 mM halothane.
†Significant difference ($p < 0.01$) between C-domain Ca^{2+} binding sites measured in 0 and 2.5 mM halothane.

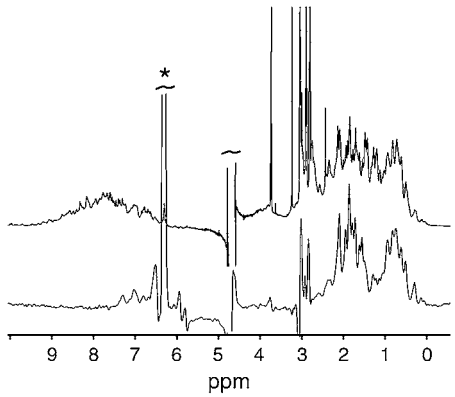

FIGURE 6 Halothane interacts predominantly with aliphatic protons in $[Ca^{2+}]_4$-CaM as determined by ^{1}HNMR. (*Top*) Trace of one-dimensional ^{1}HNMR spectrum of halothane and $[Ca^{2+}]_4$-CaM. The signal from water (4.7 ppm) is truncated. (*Bottom*) Trace from NOESY of halothane and $[Ca^{2+}]_4$-CaM, taken along the halothane resonance at 6.3 ppm, and drawn so the aliphatic regions in the upper and lower traces have approximately the same scale. The signals from water (4.7 ppm) and halothane (6.3 ppm, *asterisk*) are truncated. Appearance of signal in the aliphatic region (0–4 ppm) and the aromatic region of the spectrum (6–8 ppm) indicates spatial proximity among halothane protons and respective protein protons.

difficult to define at the molecular level. Quantifiable values that express hydrophobicity on an absolute scale, such as PW and PW_M, are easier to utilize in an approach to predict VA binding sites based on protein structure.

We found that halothane binds to $[Ca^{2+}]_4$-CaM, but not apoCaM (Fig. 3), which confirms our previous NMR work (14). We determined that the halothane·$[Ca^{2+}]_4$-CaM K_d was 1.1 mM and the ΔH was −4.2 kcal/mol, results which are consistent with VAs binding to HSA (34,51). However, we found that the magnitude of ΔS (-0.5 cal mol^{-1} K^{-1}) was as much as 20 times smaller than ΔSs measured for VA binding interactions with HSA (51), odorant binding protein (12), and an α-helix bundle protein (29). VA binding to proteins has been observed to coincide with entropy gain (12,51), as is expected for desolvation of a hydrophobic molecule and entropy loss, which was posited to result from a reduction in the mobility of protein side chains (29). The near-zero ΔS we measured for halothane·$[Ca^{2+}]_4$-CaM binding suggests that the entropy gain of halothane desolvation is counterbalanced by entropy loss in the system, such as reduced mobility of the $[Ca^{2+}]_4$-CaM side chains. This is supported by an NMR study of the dynamics of methyl group containing side chains in $[Ca^{2+}]_4$-CaM, which demonstrated that the conformational entropy of $[Ca^{2+}]_4$-CaM is reduced when it binds a peptide (52).

Structures of VA·$[Ca^{2+}]_4$-CaM complexes have yet to be determined, so the molecular interactions and binding sites are unknown. However, our experimental evidence indicates that the VA binding sites in $[Ca^{2+}]_4$-CaM are similar to those in the known structures of VA·protein complexes. We observed cross-relaxation between halothane and $[Ca^{2+}]_4$-CaM resonances within the range of 0–3 ppm and 6–8 ppm (Fig. 6). This finding is consistent with NMR experiments on halothane binding to HSA (47). Cross-relaxation indicates that a halothane molecule is bound within ~4 Å of these protein resonances. It is not possible to tell from this spectrum how many CaM resonances are involved, their assignment, or the stoichiometry of halothane in the complex. Additional isotope-edited measurements will reveal this information. They are part of an ongoing effort to determine the solution structure of halothane·$[Ca^{2+}]_4$-CaM complex, which we will report separately. However, the frequency ranges in which the cross-relaxation is observed informs us about the types of ^{1}H resonances nearby the halothane binding site(s). In general, aliphatic ^{1}H resonances are observed between 0 and 4 ppm, methyl ^{1}H resonances are observed between 0 and 3 ppm, and aromatic group ^{1}H resonances are observed between 6 and 8 ppm. The exact frequency of each resonance within these ranges depends on the local environment of the individual protons. The NOESY spectra show that the halothane binding site(s) in $[Ca^{2+}]_4$-CaM are surrounded by predominantly aliphatic and to a lesser extent aromatic ^{1}Hs, some of which are part of residues that influence VA binding (Table 1). This suggests that VAs bind within ~4 Å of residues in the sequence of $[Ca^{2+}]_4$-CaM, which are similar in type to those near VA binding sites in HSA. Thus, the molecular interactions between VAs and $[Ca^{2+}]_4$-CaM might be similar to those which we characterized in the structures of VA·protein complexes. In addition, the affinity of halothane for $[Ca^{2+}]_4$-CaM (Fig. 4) is comparable to the affinity of VAs for HSA (51), which indicates that the molecular interactions are of the same magnitude. Together, these experimental findings suggest that the molecular interactions observed in the structures of VA·protein complexes are representative of the interactions between halothane and $[Ca^{2+}]_4$-CaM. Thus, it is appropriate to use the same approach to predict VA binding sites in the structures of CaM.

BSPs in the occupancy range were found in both the extended and compact structures of $[Ca^{2+}]_4$-CaM (Fig. 1 *B*), but not in the x-ray structure of apo-CaM (Fig. 1 *B*) or in 26 of 30 NMR structures deposited for apoCaM (1LKJ, (53)) (data not shown). Thus, VAs are predicted to bind to $[Ca^{2+}]_4$-CaM, but not apoCaM. This prediction is supported by ITC (Fig. 3). The predicted binding site(s) are in the hydrophobic pockets that are present in the N- and C-domains of $[Ca^{2+}]_4$-CaM (Fig. 2). No equivalent hydrophobic pockets are present in the structure of apoCaM. The location of the predicted binding sites within these hydrophobic pockets is supported by the effect of halothane on the Ca^{2+} affinity of CaM (Fig. 5). We determined the apparent Ca^{2+} K_d values for the N- and C-domain Ca^{2+} binding sites in CaM in the absence of halothane, which agree with the findings of others (35), and found that the K_d values decrease in the presence of halothane. This finding is consistent with the effect of other VAs on the Ca^{2+} affinity of the C-domain

Ca^{2+} binding sites of CaM (37). Similar increases in the Ca^{2+} affinity of CaM have been observed in the presence of other drugs, peptides, and proteins, which bind to the hydrophobic pockets of $[Ca^{2+}]_4$-CaM (54-57). This indicates that VAs, like other hydrophobic drugs that increase the Ca^{2+} affinity of CaM, bind to the hydrophobic pockets of $[Ca^{2+}]_4$-CaM. The computational approach did not distinguish whether halothane prefers to bind to the extended or compact conformation of $[Ca^{2+}]_4$-CaM. $[Ca^{2+}]_4$-CaM has been shown to adopt a compact conformation when bound to other small hydrophobic drugs (54,58–61). However, the solution structure of the halothane·$[Ca^{2+}]_4$-CaM complex will need to be determined to verify the predicted binding sites and identify the conformation of $[Ca^{2+}]_4$-CaM in the complex.

This approach predicts VA binding sites within a protein structure, but does not indicate the orientation of the VA relative to the pocket. The location of the binding site in the protein structure could be sufficient to suggest empirical measurements to test VA occupancy of the predicted binding site. For example, VAs compete for fatty-acid binding sites and quench intrinsic tryptophan emission in serum albumin (10,21) and inhibit iron uptake, but not release in apoferritin (62). Higher-resolution predictions can be obtained using a docking algorithm to calculate the optimal orientation of a particular VA molecule in the binding site. Another group used the software AutoDock 3.0 (63) and a blind docking procedure (64) to predict halothane-binding sites in ketosteroid isomerase (KSI) dimer (65). This is a rigorous method in which binding energies are calculated for millions of unique protein·VA geometries that are intended to sample all possible binding sites on the protein. The benefits to using a docking algorithm are that it can predict the location and orientation of the bound VA and the binding energy can be used to estimate the binding affinity. The drawbacks are that the calculations require force-field parameters for the VAs and can take considerable computational time. For comparison, we used our approach to predict the VA binding sites in KSI using the same input file (1BUQ). Both our approach and the blind docking procedure identified halothane binding sites in the same pockets in the KSI dimer (data not shown). This suggests that the binding sites predicted by our approach could be used as seed locations for a focused docking algorithm. This would provide higher-resolution predictions and an estimate of affinity, while minimizing the dimensions of the search region and hence computation time. Thus, our approach predicts the location(s) of VA binding within a protein, which could be refined with the implementation of a docking algorithm.

In this work, we utilize algorithms developed to identify and characterize ligand binding sites in proteins. The efficacy of this approach suggests that it is appropriate to apply ligand binding concepts (i.e., binding sites, stoichiometry, and K_d) to VA protein interactions. This does not imply that the effects of VAs on protein function are necessarily localized to the binding site, as is thought to be the case in the competitive inhibition of luciferase by VAs (13). The effects of the VAs ligands could also delocalize over the protein structure, as suggested by a molecular dynamics simulation of the effect of halothane on a membrane-inserted channel protein (66).

This work shows that VA binding sites in the high resolution structures of VA·protein complexes correlate with descriptors of hydrophobicity (PW and PW_M) that are related to the degree to which solvent is excluded from the pocket and the number of nearby methyl groups, respectively. Thus, PW and PW_M are consistent with the observations that VA binding is driven, at least in part, by the hydrophobic effect and the Meyer-Overton rule, which indicates that VAs target hydrophobic domains. PW and PW_M can be quantified in absolute terms for high-resolution protein structures and used to predict the site(s) of VA binding in proteins, which could be a powerful tool in the study of molecular mechanisms of anesthesia. Using this approach, we predict that VAs bind to hydrophobic pockets that are present in the structures of $[Ca^{2+}]_4$-CaM, but not apoCaM. This is supported with experimental findings that VAs bind to $[Ca^{2+}]_4$-CaM, but not apo-CaM; VAs bind near predominantly aliphatic ^{1}Hs in $[Ca^{2+}]_4$-CaM, and; VAs decrease the K_d values of Ca^{2+} for CaM.

This study was supported in part by grant No. HL-45532 from the National Institutes of Health, Bethesda, Maryland and grants from Mayo Foundation, Rochester, Minnesota.

REFERENCES

1. Yokono, S., K. Ogli, S. Miura, and I. Ueda. 1989. 400 MHz two-dimensional nuclear Overhauser spectroscopy on anesthetic interaction with lipid bilayer. *Biochim. Biophys. Acta*. 982:300–302.
2. Nakagawa, T., T. Hamanaka, S. Nishimura, T. Uruga, and Y. Kito. 1994. The specific binding site of the volatile anesthetic diiodomethane to purple membrane by x-ray diffraction. *J. Mol. Biol*. 238:297–301.
3. Lopez, M. M., and D. Kosk-Kosicka. 1998. Spectroscopic analysis of halothane binding to the plasma membrane Ca^{2+}-ATPase. *Biophys. J*. 74:974–980.
4. Ishizawa, Y., R. Sharp, P. A. Liebman, and R. G. Eckenhoff. 2000. Halothane binding to a G protein coupled receptor in retinal membranes by photoaffinity labeling. *Biochemistry*. 39:8497–8502.
5. Xu, Y., T. Seto, P. Tang, and L. Firestone. 2000. NMR study of volatile anesthetic binding to nicotinic acetylcholine receptors. *Biophys. J*. 78:746–751.
6. Eckenhoff, R. G. 1996. An inhalational anesthetic binding domain in the nicotinic acetylcholine receptor. *Proc. Natl. Acad. Sci. USA*. 93: 2807–2810.
7. Xi, J., R. Liu, G. Asbury, M. Eckenhoff, and R. Eckenhoff. 2004. Inhalational anesthetic-binding proteins in rat neuronal membranes. *J. Biol. Chem*. 279:19628–19633.
8. Kai, T., K. A. Jones, and D. O. Warner. 1998. Halothane attenuates calcium sensitization in airway smooth muscle by inhibiting G-proteins. *Anesthesiology*. 89:1543–1552.
9. Franks, J. J., J. L. Horn, P. K. Janicki, and G. Singh. 1995. Halothane, isoflurane, xenon, and nitrous oxide inhibit calcium ATPase pump activity in rat brain synaptic plasma membranes. *Anesthesiology*. 82:108–117.

10. Johansson, J. S., R. G. Eckenhoff, and P. L. Dutton. 1995. Binding of halothane to serum albumin demonstrated using tryptophan fluorescence. *Anesthesiology.* 83:316–324.

11. Liu, R., P. J. Loll, and R. G. Eckenhoff. 2005. Structural basis for high-affinity volatile anesthetic binding in a natural 4-helix bundle protein. *FASEB J.* 19:567–576.

12. Johansson, J. S., G. A. Manderson, R. Ramoni, S. Grolli, and R. G. Eckenhoff. 2005. Binding of the volatile general anesthetics halothane and isoflurane to a mammalian β-barrel protein. *FEBS J.* 272:573–581.

13. Franks, N. P., A. Jenkins, E. Conti, W. R. Lieb, and P. Brick. 1998. Structural basis for the inhibition of firefly luciferase by a general anesthetic. *Biophys. J.* 75:2205–2211.

14. Streiff, J. H., N. O. Juranic, S. I. Macura, D. O. Warner, K. A. Jones, and W. J. Perkins. 2004. Saturation transfer difference nuclear magnetic resonance spectroscopy as a method for screening proteins for anesthetic binding. *Mol. Pharmacol.* 66:929–935.

15. Curry, S., W. R. Lieb, and N. P. Franks. 1990. Effects of general anesthetics on the bacterial luciferase enzyme from *Vibrio harveyi*: an anesthetic target site with differential sensitivity. *Biochemistry.* 29: 4641–4652.

16. Rebecchi, M. J., and S. N. Pentyala. 2002. Anaesthetic actions on other targets: protein kinase C and guanine nucleotide-binding proteins. *Br. J. Anaesth.* 89:62–78.

17. Hemmings, H. C., Jr. 1998. General anesthetic effects on protein kinase C. *Toxicol. Lett.* 100–101:89–95.

18. Slater, S. J., M. B. Kelly, J. D. Larkin, C. Ho, A. Mazurek, F. J. Taddeo, M. D. Yeager, and C. D. Stubbs. 1997. Interaction of alcohols and anesthetics with protein kinase C-α. *J. Biol. Chem.* 272:6167–6173.

19. Pentyala, S. N., K. Sung, A. Chowdhury, and M. J. Rebecchi. 1999. Volatile anesthetics modulate the binding of guanine nucleotides to the α-subunits of heterotrimeric GTP binding proteins. *Eur. J. Pharmacol.* 384:213–222.

20. Eckenhoff, R. G., J. W. Tanner, and P. A. Liebman. 2001. Cooperative binding of inhaled anesthetics and ATP to firefly luciferase. *Proteins.* 42:436–441.

21. Dubois, B. W., and A. S. Evers. 1992. 19F-NMR spin-spin relaxation (T2) method for characterizing volatile anesthetic binding to proteins. Analysis of isoflurane binding to serum albumin. *Biochemistry.* 31: 7069–7076.

22. Bhattacharya, A. A., S. Curry, and N. P. Franks. 2000. Binding of the general anesthetics propofol and halothane to human serum albumin. High resolution crystal structures. *J. Biol. Chem.* 275:38731–38738.

23. Moss, G. W., N. P. Franks, and W. R. Lieb. 1991. Modulation of the general anesthetic sensitivity of a protein: a transition between two forms of firefly luciferase. *Proc. Natl. Acad. Sci. USA.* 88:134–138.

24. Schumacher, M. A., M. Crum, and M. C. Miller. 2004. Crystal structures of apocalmodulin and an apocalmodulin/SK potassium channel gating domain complex. *Structure.* 12:849–860.

25. Chattopadhyaya, R., W. E. Meador, A. R. Means, and F. A. Quiocho. 1992. Calmodulin structure refined at 1.7 Å resolution. *J. Mol. Biol.* 228:1177–1192.

26. Fallon, J. L., and F. A. Quiocho. 2003. A closed compact structure of native Ca^{2+}-calmodulin. *Structure.* 11:1303–1307.

27. Marley, J., M. Lu, and C. Bracken. 2001. A method for efficient isotopic labeling of recombinant proteins. *J. Biomol. NMR.* 20:71–75.

28. Putkey, J. A., G. R. Slaughter, and A. R. Means. 1985. Bacterial expression and characterization of proteins derived from the chicken calmodulin cDNA and a calmodulin processed gene. *J. Biol. Chem.* 260:4704–4712.

29. Zhang, T., and J. J. Johansson. 2003. An isothermal titration calorimetry study on the binding of four volatile anesthetics to the hydrophobic core of a four-α-helix bundle protein. *Biophys. J.* 85:1–7.

30. Tanner, J. W. 2003. Weak binding thermodynamic parameter determination using isothermal titration calorimetry: a general method. 2003 Current Trends in Microcalorimetry. Boston, MA. http://www.microcalorimetry.com/index.php?id=182.

31. Van Dyke, R. A., and C. L. Wood. 1973. Binding of radioactivity from 14 C-labeled halothane in isolated perfused rat livers. *Anesthesiology.* 38:328–332.

32. Wiseman, T., S. Williston, J. F. Brandts, and L. N. Lin. 1989. Rapid measurement of binding constants and heats of binding using a new titration calorimeter. *Anal. Biochem.* 179:131–137.

33. Dubois, B. W., S. F. Cherian, and A. S. Evers. 1993. Volatile anesthetics compete for common binding sites on bovine serum albumin: a 19F-NMR study. *Proc. Natl. Acad. Sci. USA.* 90:6478–6482.

34. Sawas, A. H., S. N. Pentyala, and M. J. Rebecchi. 2004. Binding of volatile anesthetics to serum albumin: measurements of enthalpy and solvent contributions. *Biochemistry.* 43:12675–12685.

35. VanScyoc, W. S., B. R. Sorensen, E. Rusinova, W. R. Laws, J. B. Ross, and M. A. Shea. 2002. Calcium binding to calmodulin mutants monitored by domain-specific intrinsic phenylalanine and tyrosine fluorescence. *Biophys. J.* 83:2767–2780.

36. VanScyoc, W. S., and M. A. Shea. 2001. Phenylalanine fluorescence studies of calcium binding to N-domain fragments of *Paramecium* calmodulin mutants show increased calcium affinity correlates with increased disorder. *Protein Sci.* 10:1758–1768.

37. Levin, A., and T. J. Blanck. 1995. Halothane and isoflurane alter the Ca^{2+} binding properties of calmodulin. *Anesthesiology.* 83:120–126.

38. Bosterling, B., A. Trevor, and J. R. Trudell. 1982. Binding of halothane-free radicals to fatty acids following UV irradiation. *Anesthesiology.* 56:380–384.

39. Macura, S., and R. R. Ernst. 1980. Elucidation of cross-relaxation in liquids by two-dimensional NMR spectroscopy. *Mol. Phys.* 41:95–117.

40. Bourne, P. E., K. J. Addess, W. F. Bluhm, L. Chen, N. Deshpande, Z. Feng, W. Fleri, R. Green, J. C. Merino-Ott, W. Townsend-Merino, H. Weissig, J. Westbrook, and H. M. Berman. 2004. The distribution and query systems of the RCSB Protein Data Bank. *Nucleic Acids Res.* 32:D223–D225.

41. Granier, T., B. Gallois, A. Dautant, B. Langlois-D'Estaintot, and G. Precigoux. 1997. Comparison of the structures of the cubic and tetragonal forms of horse-spleen apoferritin. *Acta Crystallogr. D Biol. Chrystallogr.* 53:580–587.

42. Humphrey, W., A. Dalke, and K. Schulten. 1996. VMD—visual molecular dynamics. *J. Mol. Graph.* 14:33–38.

43. Kalé, L., R. Skeel, M. Bhandarkar, R. Brunner, A. Gursoy, N. Krawetz, J. Phillips, A. Shinozaki, K. Varadarajan, and K. Schulten. 1999. NAMD2: greater scalability for parallel molecular dynamics. *J. Comput. Phys.* 151:283–312.

44. Brady, G. P., Jr., and P. F. Stouten. 2000. Fast prediction and visualization of protein binding pockets with PASS. *J. Comput. Aided Mol. Des.* 14:383–401.

45. Liu, R., R. Pidikiti, C. E. Ha, C. E. Petersen, N. V. Bhagavan, and R. G. Eckenhoff. 2002. The role of electrostatic interactions in human serum albumin binding and stabilization by halothane. *J. Biol. Chem.* 277:36373–36379.

46. Liu, R., and R. G. Eckenhoff. 2005. Weak polar interactions confer albumin binding site selectivity for haloether anesthetics. *Anesthesiology.* 102:799–805.

47. Shikii, K., S. Sakurai, H. Utsumi, H. Seki, and M. Tashiro. 2004. Application of the 19F NMR technique to observe binding of the general anesthetic halothane to human serum albumin. *Anal. Sci.* 20:1475–1477.

48. Overton, E. 1901. Studies on Anesthesia with a Report on General Pharmacology. Gustav Fischer, Jena, Germany.

49. Meyer, H. 1899. Which aspect of anesthetics causes its narcotic effect? *Naunyn Schmiedebergs Arch. Exp. Pathol. Pharmakol.* 42:109–118.

50. Otting, G., E. Liepinsh, B. Halle, and U. Frey. 1997. NMR identification of hydrophobic cavities with low water occupancies in protein structures using small gas molecules. *Nat. Struct. Biol.* 4:396–404.

51. Liu, R., Q. Meng, J. Xi, J. Yang, C. E. Ha, N. V. Bhagavan, and R. G. Eckenhoff. 2004. Comparative binding character of two general anaesthetics for sites on human serum albumin. *Biochem. J.* 380: 147–152.

52. Lee, A. L., S. A. Kinnear, and A. J. Wand. 2000. Redistribution and loss of side chain entropy upon formation of a calmodulin-peptide complex. *Nat. Struct. Biol.* 7:72–77.

53. Ishida, H., K. Nakashima, Y. Kumaki, M. Nakata, K. Hikichi, and M. Yazawa. 2002. The solution structure of apocalmodulin from *Saccharomyces cerevisiae* implies a mechanism for its unique Ca^{2+} binding property. *Biochemistry.* 41:15536–15542.

54. Massom, L., H. Lee, and H. W. Jarrett. 1990. Trifluoperazine binding to porcine brain calmodulin and skeletal muscle troponin C. *Biochemistry.* 29:671–681.

55. Ohashi, I., R. Pohoreki, K. Morita, and P. M. Stemmer. 2004. Alcohols increase calmodulin affinity for Ca^{2+} and decrease target affinity for calmodulin. *Biochim. Biophys. Acta.* 1691:161–167.

56. Peersen, O. B., T. S. Madsen, and J. J. Falke. 1997. Intermolecular tuning of calmodulin by target peptides and proteins: differential effects on Ca^{2+} binding and implications for kinase activation. *Protein Sci.* 6:794–807.

57. Mirzoeva, S., S. Weigand, T. J. Lukas, L. Shuvalova, W. F. Anderson, and D. M. Watterson. 1999. Analysis of the functional coupling between calmodulin's calcium binding and peptide recognition properties. *Biochemistry.* 38:3936–3947.

58. Craven, C. J., B. Whitehead, S. K. Jones, E. Thulin, G. M. Blackburn, and J. P. Waltho. 1996. Complexes formed between calmodulin and the antagonists J-8 and TFP in solution. *Biochemistry.* 35:10287–10299.

59. Matsushima, N., N. Hayashi, Y. Jinbo, and Y. Izumi. 2000. Ca^{2+}-bound calmodulin forms a compact globular structure on binding four trifluoperazine molecules in solution. *Biochem. J.* 347:211–215.

60. Osawa, M., M. B. Swindells, J. Tanikawa, T. Tanaka, T. Mase, T. Furuya, and M. Ikura. 1998. Solution structure of calmodulin-W-7 complex: the basis of diversity in molecular recognition. *J. Mol. Biol.* 276:165–176.

61. Osawa, M., S. Kuwamoto, Y. Izumi, K. L. Yap, M. Ikura, T. Shibanuma, H. Yokokura, H. Hidaka, and N. Matsushima. 1999. Evidence for calmodulin inter-domain compaction in solution induced by W-7 binding. *FEBS Lett.* 442:173–177.

62. West, J., J. Xi, R. Liu, I. Dmochowski, and R. G. Eckenhoff. 2005. Volatile anesthetics reduce iron uptake by apoferritin. American Society of Anesthesiologists. Atlanta, GA.

63. Morris, G. M., D. S. Goodsell, R. S. Halliday, R. Huey, W. E. Hart, R. K. Belew, and A. J. Olson. 1998. Automated docking using a Lamarckian genetic algorithm and an empirical binding free energy function. *J. Comput. Chem.* 19:1639–1662.

64. Hetenyi, C., and D. van der Spoel. 2002. Efficient docking of peptides to proteins without prior knowledge of the binding site. *Protein Sci.* 11:1729–1737.

65. Yonkunas, M. J., Y. Xu, and P. Tang. 2005. Anesthetic interaction with ketosteroid isomerase: insights from molecular dynamics simulations. *Biophys. J.* 89:2350–2356.

66. Tang, P., and Y. Xu. 2002. Large-scale molecular dynamics simulations of general anesthetic effects on the ion channel in the fully hydrated membrane: the implication of molecular mechanisms of general anesthesia. *Proc. Natl. Acad. Sci. USA.* 99:16035–16040.